1

Data-Driven Modeling in Geomechanics

Konstantinos KARAPIPERIS
ETH Zürich, Switzerland

The theoretical framework of data-driven computational mechanics presents an alternative formulation of mechanics, whereby optimal material states are sought within a dataset that most closely satisfies momentum and energy conservation principles. We review the framework for the case of simple and non-simple (polar), elastic and inelastic media, which represent common descriptions for geomaterials. Data mining from experiments and high-fidelity lower scale simulations (DEM and FEM) are discussed, while remedies for data scarcity (adaptive data sampling) are also highlighted. Representative examples of a flat punch indentation and a rupture through a soil layer are presented, and a link to open-source Python code is provided.

For a color version of all the figures in this chapter, see www.iste.co.uk/stefanou/machine2.zip.

Machine Learning in Geomechanics 2,
coordinated by Ioannis STEFANOU and Félix DARVE.

1.1. Introduction

Predictive models in geomechanics have traditionally relied on continuum modeling via the formulation constitutive equations (Darve and Labanieh 1982; Mühlhaus and Alfantis 1991; Vardoulakis and Aifantis 1991; Ortiz and Pandolfi 2004; Dafalias and Manzari 2004; Darve and Nicot 2005; Borja and Andrade 2006; Houlsby and Puzrin 2006), discrete particle-based models (Cundall and Strack 1979; Bardet 1994; Kawamoto et al. 2018) and multiscale techniques that bridge the continuum and discrete scales (Christoffersen et al. 1981; Nicot et al. 2005; Kamrin et al. 2007; Andrade and Tu 2009; Guo and Zhao 2014; Regueiro and Yan 2011). Initially informed by macroscopic experiments (Roscoe et al. 1958; Roscoe 1970), and later by high-fidelity grain-scale resolved experiments (Hall et al. 2010; Andò et al. 2012), these models have been successful in capturing essential aspects of granular materials and, more generally, geomaterials including pressure-dependent elasticity, history dependence and critical state, fabric evolution and non-locality. Despite their success, further progress has been hindered by numerous challenges including the uncertainty related to the models at different scales, as well as their complexity and the associated laborious process of calibration.

Recently, a variety of data-driven approaches have been developed in order to tackle the challenges outlined above, most importantly the bias, complexity or inefficiency of these methods, while incorporating information about the underlying mechanics and physics. These include physics-informed neural networks (Haghighat et al. 2021) with a built-in structure of elastoplasticity (Eghbalian et al. 2022; Haghighat et al. 2023; Vlassis and Sun 2023), or with incorporated thermodynamics constraints (Masi et al. 2021; Huang et al. 2022). Despite the physical basis of these models, they are often hard to interpret and could suffer from generalization errors for unseen stress–strain paths. An alternative approach that is not based on learning a constitutive law, but rather relies directly on the raw data, is furnished by the framework of data-driven computational mechanics (DDCM), introduced by Ortiz and co-workers. In DDCM, the mechanical problem is reformulated in terms of distances between a

material dataset obtained from experiments, and an equilibrium set where the states that satisfy the physics reside. The method has been extended in various directions, including inelasticity (Eggersmann et al. 2019), non-locality (Karapiperis et al. 2021), stochasticity (Prume et al. 2023), fracture (Carrara et al. 2020) and breakage mechanics (Ulloa et al. 2023), and has been coupled with model-based approaches (Bahmani and Sun 2021) and machine-learning techniques (Eggersmann et al. 2021; Bahmani and Sun 2022) in an effort to boost the efficiency and robustness of the method. The source of the data can be experiments (Leygue et al. 2018) or high-fidelity micromechanical calculations (Karapiperis et al. 2020b).

The chapter is organized as follows. In section 1.2.1, the framework of data-driven mechanics is presented for simple continua, which is then extended to micropolar continua with a microstructure in section 1.2.2. The enhancement of the framework to inelasticity is addressed in section 1.2.3. Then, the source of data (experiments and micromechanical simulations) is discussed (section 1.2.4), focusing also on data scarcity and how it can be efficiently overcome. We conclude with representative examples and a link to an open-source code repository (section 1.3).

1.2. Data-driven computational mechanics

1.2.1. *Cauchy continuum – elasticity*

Let us first restrict our attention to the geometrically linear mechanical problem of a *simple* (nonlinear) elastic body that is discretized into N nodes and M material points (Figure 1.1). The body is subject to applied forces $\mathbf{f} = \{\mathbf{f}^\alpha\}_{\alpha=1}^N$ and undergoes displacements $\mathbf{u} = \{\mathbf{u}^\alpha\}_{\alpha=1}^N$ at its nodes. The state of each material point is described by a stress–strain pair indicating a point in the local phase space, that is, $\mathbf{z}^e = (\boldsymbol{\varepsilon}^e, \boldsymbol{\sigma}^e) \in Z^e$, and the state of the entire system is collectively a point in the global phase space $\mathbf{z} = \{\mathbf{z}^e\}_{e=1}^M \in Z$. The system is subject to the following discretized compatibility and equilibrium constraints:

$$\varepsilon_{ij}^{e} = \frac{1}{2}\sum_{\alpha}\left(N_{,j}^{e\alpha}u_{i}^{\alpha} + N_{,i}^{e\alpha}u_{j}^{\alpha}\right), \qquad e = 1,\ldots,M \qquad [1.1]$$

$$\sum_{e=1}^{M} w_e \sigma_{ij}^{e} N_{,j}^{e\alpha} = f_{i}^{\alpha}, \qquad \alpha = 1,\ldots,N \qquad [1.2]$$

where N^{ea} is the shape function of node α evaluated at the material point e within a finite element approximation scheme, and $\{w_e\}_{e=1}^{M}$ are elements of volume. The set of global states satisfying the above constraints define the equilibrium set E.

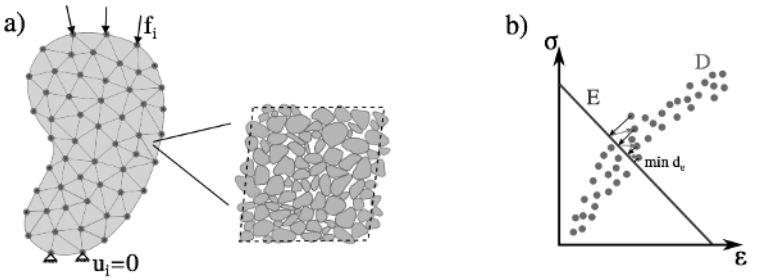

Figure 1.1. *(a) Simple continuum with granular microstructure. (b) Illustration of the stress–strain states in the material dataset (D) and their projections on the equilibrium set (E) with highlighted iterative procedure leading to a minimum distance solution*

Instead of relying on a constitutive relation of the form $\boldsymbol{\sigma}^{e} = \boldsymbol{\sigma}^{e}(\boldsymbol{\varepsilon}^{e})$ for closure, the data-driven formulation of the problem consists of finding the global state $\mathbf{z}$ that satisfies the compatibility and equilibrium constraints and, at the same time, minimizes the distance to a given material dataset D. Therefore, the local phase spaces Z_e are equipped with an appropriate metric:

$$|\mathbf{z}^{e}| = \mathbb{C}^{e}\,\boldsymbol{\varepsilon}^{e}\cdot\boldsymbol{\varepsilon}^{e} + \mathbb{C}^{e^{-1}}\boldsymbol{\sigma}^{e}\cdot\boldsymbol{\sigma}^{e} \qquad [1.3]$$

where $\mathbb{C}^{e}$ is a symmetric positive-definite tensor. Although the purpose of this tensor is numerical, and does not represent actual material behavior, it is typically given as the isotropic linear elasticity tensor:

$$\mathbb{C}_{ijkl}^{e} = \lambda\delta_{ij}\delta_{kl} + \mu(\delta_{ik}\delta_{jl} + \delta_{il}\delta_{jk}) \qquad [1.4]$$

Note that this introduces two parameters λ, μ to the problem, the choice of which may generally affect how well the compatibility or equilibrium constraints are satisfied. To avoid this issue, and at the same time, obtain a parameter-free scheme, one can alternatively introduce a nested optimization problem within the definition of the distance as follows (e.g. Karapiperis et al. (2021)):

$$|\mathbf{z}^e| = \min_{\lambda,\mu>0} \mathbb{C}^e(\lambda,\mu)\,\boldsymbol{\varepsilon}^e \cdot \boldsymbol{\varepsilon}^e + \mathbb{C}^{e^{-1}}(\lambda,\mu)\boldsymbol{\sigma}^e \cdot \boldsymbol{\sigma}^e \qquad [1.5]$$

In the following, we will assume that a constant $\mathbb{C}^e$ is used, for the definition of the distance in the phase space. As a result, a metrization of the global phase space Z is induced by means of the norm:

$$|\mathbf{z}| = \sum_{e=1}^{N} w_e |\mathbf{z}^e|$$

The problem is mathematically formulated as:

$$\min_{\mathbf{y}\in D} \min_{\mathbf{z}\in E} |\mathbf{z} - \mathbf{y}| \qquad [1.6]$$

where z denotes the *mechanical state* of the system, that is, the set of stress–strain pairs that satisfy equilibrium and compatibility, and y denotes the *material state* of the system, that is, the set of stress–strain pairs in the dataset.

The compatibility constraints are imposed by means of direct substitution, while the equilibrium constraints are enforced using Lagrange multipliers, resulting in the stationary problem:

$$\delta \Bigg[\sum_e w^e |z^e| \big(\frac{1}{2} \sum_\alpha \big(N^{e\alpha}_{,j} u^\alpha_i + N^{e\alpha}_{,i} u^\alpha_j\big), \sigma^e_{ij}\big) - \sum_\alpha \big(\sum_e w_e \sigma^e_{ij} N^{e\alpha}_{,j} - f^\alpha_i \big) \eta^\alpha_i \Bigg] = 0 \qquad [1.7]$$

Taking all possible variations $(\delta u_i^\alpha, \delta\sigma_{ij}^e, \delta\eta_i^a)$, and manipulating the resulting equations, we obtain a system of Euler–Lagrange equations (Kirchdoerfer and Ortiz 2016):

$$\sum_b \sum_e w_e C_{ijkl}^{e^*} N_{,j}^{e\alpha} N_{,l}^{eb} u_k^b = \sum_e w_e C_{ijkl}^{e^*} N_{,j}^{e\alpha} \varepsilon_{kl}^{e^*} \qquad [1.8]$$

$$\sum_b \sum_e w_e C_{ijkl}^{e^*} N_{,j}^{e\alpha} N_{,l}^{eb} \eta_k^b = f_i^\alpha - \sum_e w_e N_{,j}^{e\alpha} \sigma_{ij}^{e^*} \qquad [1.9]$$

where $\mathbf{z}^{e^*} = (\boldsymbol{\varepsilon}^{e^*}, \boldsymbol{\sigma}^{e^*})$ are the optimal local data points in the dataset D^e that result in the closest possible satisfaction of the constraints. Equations [1.8] and [1.9] represent two standard linear elasticity problems, one in terms of $\mathbf{u}$ and another in terms of $\boldsymbol{\eta}$.

Solution algorithm

Note that the optimal local points $\mathbf{y}^e = (\boldsymbol{\varepsilon}^{e^*}, \sigma^{e^*})$ in the dataset D^e are not known a priori, which therefore calls for an iterative solution scheme. The simplest algorithm involves a fixed point iteration, where a fixed material state $\mathbf{y}^{(k)}$ is projected onto E (i.e. equations [1.8] and [1.9] are solved) to obtain the updated mechanical state $\mathbf{z}^{(k)}$, where k denotes the iteration number. Then a search through the dataset is carried out to find the closest material state $\mathbf{y}^{(k+1)}$, and the process is repeated until the material states remain unchanged. For more details, the interested reader is referred to some previous studies (Kirchdoerfer and Ortiz 2016; Karapiperis et al. 2020b).

1.2.2. *Micropolar continuum – elasticity*

The simple or Cauchy continuum is known to have limitations when it comes to modeling geomaterials, especially in the failure regime (shear localization). due to the absence of an internal length scale (Mühlhaus and Vardoulakis 1987). In this section, we describe the extension of the data-driven computational mechanics framework to the micropolar continuum, following (Karapiperis et al. 2021). We therefore proceed to consider the mechanical problem of a (nonlinear) elastic micropolar body that is discretized into N nodes and M material points, similar to section 1.2.1. However, the body is now

subject to not only applied forces $\mathbf{f} = \{\mathbf{f}^\alpha\}_{\alpha=1}^N$ but also moments $\mathbf{m} = \{\mathbf{m}^\alpha\}_{\alpha=1}^N$ (Figure 1.2). Its kinematics are described by displacements $\mathbf{u} = \{\mathbf{u}^\alpha\}_{\alpha=1}^N$ and microrotations $\boldsymbol{\theta} = \{\theta^\alpha\}_{\alpha=1}^N$ at its nodes. Analogously, the state of each material point is described by a stress–strain pair $(\boldsymbol{\varepsilon}^e, \boldsymbol{\sigma}^e)$ and couple stress–curvature pair $(\boldsymbol{\kappa}^e, \boldsymbol{\mu}^e)$, which all together constitute a point in the local phase space, that is, $\mathbf{z}^e = (\boldsymbol{\varepsilon}^e, \boldsymbol{\kappa}^e, \boldsymbol{\sigma}^e, \boldsymbol{\mu}^e)$, and the state of the entire system is collectively a point in the global phase space $\mathbf{z} = \{\mathbf{z}^e\}_{e=1}^M \in Z$. The micropolar system is subject to the following discretized compatibility and equilibrium constraints:

$$\varepsilon_{ij}^e = \sum_\alpha \left(N_{,j}^{e\alpha} u_i^\alpha + \epsilon_{ijk} N^{e\alpha} \theta_k^\alpha\right), \qquad e = 1, \ldots, M \qquad [1.10]$$

$$\kappa_{ij}^e = \sum_\alpha N_{,j}^{e\alpha} \theta_i^\alpha, \qquad e = 1, \ldots, M \qquad [1.11]$$

$$\sum_{e=1}^M w_e \sigma_{ij}^e N_{,j}^{e\alpha} = f_i^\alpha, \qquad \alpha = 1, \ldots, N \qquad [1.12]$$

$$\sum_{e=1}^M w_e \left(\mu_{ij}^e N_{,j}^{e\alpha} + \epsilon_{ijk} \sigma_{jk}^e N^{e\alpha}\right) = m_i^\alpha, \alpha = 1, \ldots, N \qquad [1.13]$$

where, besides the quantities already introduced in section 1.2.1, ϵ_{ijk} is the third-order permutation tensor. The set of global states satisfying the above constraints defines the equilibrium set E.

Analogously, we assume that a dataset D is available, where material states reside. The micropolar formulation of the data-driven problem involves finding the global state $\mathbf{z}$ that satisfies the compatibility and equilibrium constraints and, at the same time, minimizes the distance to the material dataset. To this end, we shall extend the metric introduced in the Cauchy continuum to account for the additional kinematic and conjugate kinetic measures present in the micropolar continuum:

$$|\mathbf{z}^e| = \mathbb{C}^e\, \boldsymbol{\varepsilon}^e \cdot \boldsymbol{\varepsilon}^e + \mathbb{D}^e\, \boldsymbol{\kappa}^e \cdot \boldsymbol{\kappa}^e + \mathbb{C}^{e^{-1}} \boldsymbol{\sigma}^e \cdot \boldsymbol{\sigma}^e + \mathbb{D}^{e^{-1}}\, \boldsymbol{\mu}^e \cdot \boldsymbol{\mu}^e \qquad [1.14]$$

where $\mathbb{C}^e$, $\mathbb{D}^e$ are the isotropic micropolar elasticity tensors, which once again do not reflect actual material properties, but are introduced for solely distance-inducing purposes:

$$\mathbb{C}^e_{ijkl} = \lambda\delta_{ij}\delta_{kl} + (\mu+\kappa)\delta_{ik}\delta_{jl} + (\mu-\kappa)\delta_{il}\delta_{jk} \quad [1.15]$$

$$\mathbb{D}^e_{ijkl} = \alpha\delta_{ij}\delta_{kl} + (\gamma+\beta)\delta_{ik}\delta_{jl} + (\gamma-\beta)\delta_{il}\delta_{jk} \quad [1.16]$$

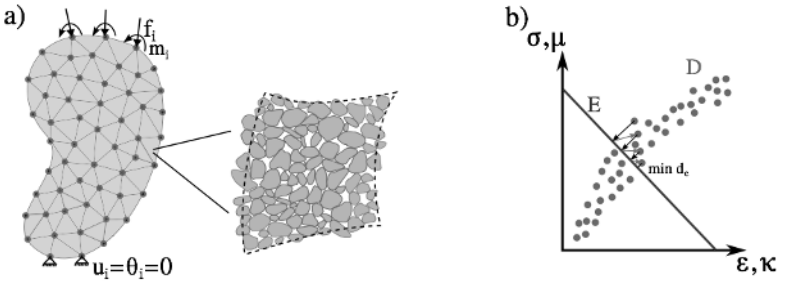

Figure 1.2. *(a) Micropolar continuum with granular microstructure. (b) Illustration of the stress–strain states in the material dataset (D) and their projections on the equilibrium set (E) with highlighted iterative procedure leading to a minimum distance solution*

The data-driven problem retains the same mathematical formulation as in the Cauchy problem:

$$\min_{\mathbf{y}\in D}\min_{\mathbf{z}\in E}|\mathbf{z}-\mathbf{y}| \quad [1.17]$$

with the difference that the state space has higher dimensions due to the presence of the additional conjugate quantities related to the field of microrotations.

The stationary problem reads:

$$\delta\Bigg[\sum_e w^e|z^e|\Big(\sum_\alpha N^{e\alpha}_{,j}u^\alpha_i \quad [1.18]$$

$$+\sum_\alpha \epsilon_{ijk}N^{e\alpha}\theta^\alpha_k, \sum_\alpha N^{e\alpha}_{,j}\theta^\alpha_i, \sigma^e_{ij}, \mu^e_{ij}\Big)$$

$$- \sum_{\alpha} \Big(\sum_{e} w_e \sigma_{ij}^{e} N_{,j}^{e\alpha} - f_i^{\alpha} \Big) \eta_i^{\alpha}$$

$$- \sum_{\alpha} \Big(\sum_{e} w_e (\mu_{ij}^{e} N_{,j}^{e\alpha} + \epsilon_{ijk} \sigma_{jk}^{e} N^{e\alpha}) - m_i^{\alpha} \Big) \zeta_i^{\alpha} \Bigg] = 0$$

Taking all possible variations $(\delta u_i^{\alpha}, \delta \theta_i^{\alpha}, \delta \sigma_{ij}^{e}, \delta \mu_{ij}^{e}, \delta \eta_i^{a}, \delta \zeta_i^{a})$, we obtain the following system of coupled Euler–Lagrange equations:

$$\sum_{b} \sum_{e} w_e \big(C_{ijkl}^{e} N_{,j}^{e\alpha} N_{,l}^{eb} u_k^{b} + C_{ijkl}^{e} N_{,j}^{e\alpha} N^{eb} \epsilon_{klm} \theta_m^{b} \big)$$

$$= \sum_{e} w_e C_{ijkl}^{e^*} N_{,j}^{e\alpha} \varepsilon_{kl}^{e^*} \qquad [1.19]$$

$$\sum_{b} \sum_{e} w_e \big[C_{ijkl}^{e} N^{e\alpha} N_{,l}^{eb} \epsilon_{ijm} u_k^{b} + \big(C_{ijkl}^{e} \epsilon_{ijm} \epsilon_{kln} N^{e\alpha} N^{eb}$$

$$+ D_{mjnl}^{e^*} N_{,j}^{e\alpha} N_{,l}^{eb} \big) \theta_n^{b} \big]$$

$$= \sum_{e} w_e \big(C_{ijkl}^{e} \epsilon_{ijm} N^{e\alpha} \epsilon_{kl}^{e^*} + D_{mjkl}^{e} N_{,j}^{e\alpha} \kappa_{kl}^{e^*} \big) \qquad [1.20]$$

$$\sum_{b} \sum_{e} w_e \big(C_{ijkl}^{e} N_{,j}^{eb} N_{,l}^{e\alpha} \eta_i^{b} + C_{ijkl}^{e} N^{eb} N_{,l}^{e\alpha} \epsilon_{kij} \zeta_k^{b} \big)$$

$$= f_k^{\alpha} - \sum_{e} w_e N_{,l}^{e\alpha} \sigma_{kl}^{e^*} \qquad [1.21]$$

$$\sum_{b} \sum_{e} w_e \big[C_{ijkl}^{e} N^{e\alpha} N_{,l}^{eb} \epsilon_{ijm} \eta_k^{b} + \big(C_{ijkl}^{e} \epsilon_{ijm} \epsilon_{kln} N^{e\alpha} N^{eb}$$

$$+ D_{mjnl}^{e} N_{,j}^{e\alpha} N_{,l}^{eb} \big) \zeta_n^{b} \big]$$

$$= m_m^{\alpha} - \sum_{e} w_e \big(N_{,l}^{e\alpha} \mu_{ml}^{e^*} + \epsilon_{mkl} N^{e\alpha} \sigma_{kl}^{e^*} \big) \qquad [1.22]$$

where $\mathbf{z}^{e^*} = (\boldsymbol{\varepsilon}^{e^*}, \boldsymbol{\kappa}^{e^*}, \boldsymbol{\sigma}^{e^*}, \boldsymbol{\mu}^{e^*})$ are the optimal local data points in the dataset D^e that result in the closest possible satisfaction of the constraints. Equations [1.19] and [1.20] and [1.21] and [1.22] represent two micropolar linear elasticity problems, one in terms of $\mathbf{u}, \boldsymbol{\theta}$ and another in terms of $\boldsymbol{\eta}, \boldsymbol{\zeta}$.

1.2.3. *Extension to inelasticity*

Practical applications in geomechanics often concern deformations beyond the elastic regime, which involve history dependence and irreversibility. For conciseness, we will present the extension to inelasticity for the Cauchy problem, but the inelastic extension for the micropolar problem follows analogously (Karapiperis et al. 2021). To this end, we attend to a time-discrete formulation, whereby the data-driven problem of at time t_{k+1} reads:

$$\min_{\mathbf{y}_{k+1}\in D_{k+1}} \min_{\mathbf{z}_{k+1}\in E_{k+1}} |\mathbf{z}_{k+1} - \mathbf{y}_{k+1}| \qquad [1.23]$$

where $\mathbf{z}_{k+1} = \{\mathbf{z}^e_{k+1}\}_{e=1}^M \in Z$ and $\mathbf{z}^e_{k+1} = (\boldsymbol{\varepsilon}^e_{k+1}, \boldsymbol{\sigma}^e_{k+1})$. The time-dependent constraint set E_{k+1} arises from the time-dependent applied forces $\mathbf{f}_{k+1}$. Accordingly, the behavior at a material point is described by a material dataset D^e_{k+1} of points that is attainable at time t_{k+1} given its past local history of deformation:

$$D^e_{k+1} = \{(\boldsymbol{\varepsilon}^e_{k+1}, \boldsymbol{\sigma}^e_{k+1}) \,|\, \text{past history}\} \qquad [1.24]$$

In practical terms, this implies that one has to deal with evolving material datasets. The conceptually simplest yet computationally expensive parameterization of the history relies on keeping a (potentially truncated) memory of the strain history at a material point (Eggersmann et al. 2019). This mathematically translates to:

$$D^e_{k+1} = \{(\boldsymbol{\varepsilon}^e_{k+1}, \boldsymbol{\sigma}^e_{k+1}) \,|\, \{\boldsymbol{\varepsilon}^e_l\}_{l\leq k}\} \qquad [1.25]$$

which resembles a data-driven formulation focusing on trajectories – rather than points – in stress–strain space.

An alternative approach relies on enhancing the state space with a suitable set of internal variables $\boldsymbol{q}$, which represent the evolving internal structure of the material at hand, and encapsulates its history (Karapiperis et al. 2020b; Eggersmann et al. 2019). In this case, the material dataset admits the parameterization:

$$D^e_{k+1} = \{(\boldsymbol{\varepsilon}^e_{k+1}, \boldsymbol{\sigma}^e_{k+1}) \,|\, (\boldsymbol{\varepsilon}^e_k, \boldsymbol{\sigma}^e_k, \boldsymbol{q}^e_k)\} \qquad [1.26]$$

The internal variable parametrization outlined above can be replaced or enhanced with an energy-based parametrization, whereby the state space is augmented with the free energy $\mathcal{A}$ and dissipation $\mathcal{D}$, which are related to the state variables $\boldsymbol{\epsilon}, \boldsymbol{\sigma}$ via the principle of conservation of energy and the second principle (Clausius–Plank inequality), stated in a time-discrete setting as:

$$\mathcal{D}^e_{k+1} - \mathcal{D}^e_k = \frac{\boldsymbol{\sigma}^e_k + \boldsymbol{\sigma}^e_{k+1}}{2} : (\boldsymbol{\epsilon}^e_{k+1} - \boldsymbol{\epsilon}^e_k) - (\mathcal{A}^e_{k+1} - \mathcal{A}^e_k) \geq 0 \quad [1.27]$$

The local material dataset at time t_{k+1} is then represented as:

$$D^e_{k+1} = \{(\boldsymbol{\epsilon}^e_{k+1}, \boldsymbol{\sigma}^e_{k+1}) \,|\, (\boldsymbol{\epsilon}^e_k, \boldsymbol{\sigma}^e_k), (1.27)\} \quad [1.28]$$

The above relation states that the admissible stress–strain pairs at time t_{k+1} are those that are thermodynamically consistent with the material state at time t_k. The special case where $\mathcal{D}^e_{k+1} - \mathcal{D}^e_k = 0$ defines a bounded equilibrium set (or elastic domain) on the augmented state space. More details about the various options for history parametrization can be found in some previous studies (Eggersmann et al. 2019; Karapiperis et al. 2020b). Note that in the case of the internal variable and energy-based parameterization, the necessary quantities can be obtained directly from lower scale models, for example, as we will address in section 1.2.4.

Regardless of the particular choice of parameterization of the local material datasets, the global material dataset then follows as:

$$D_{k+1} = D^1_{k+1} \times \ldots \times D^M_{k+1} \quad [1.29]$$

1.2.4. *Data sampling*

So far, we have assumed that material data are available, but we have not addressed the source of the data or their potential scarcity. In principle, data can be obtained from various sources, either experimental or computational, and potentially combined within the same simulation. The experimental identification of material datasets has been addressed in Leygue et al. (2018), whereby a database of

stress–strain couples is compiled from a given displacement field – obtained though imaging techniques – and known boundary conditions by solving a distance minimization problem (Figure 1.3(a)). Alternatively, data can be compiled from high-fidelity lower scale simulations (Karapiperis et al. 2020b), which for geomechanical problems typically amount to discrete element models in case of granular assemblies, or finite element models of heterogeneous porous materials (Figure 1.3(b)). This approach gives rise a multiscale interpretation of data-driven computing. In the latter case, homogenization principles shall be used to derive the macroscopic quantities that describe the material states (stress, structural variables and energetical quantities). These principles are reviewed below in the case of discrete assemblies (e.g. granular media) and continuum representative volume elements (e.g. porous rocks).

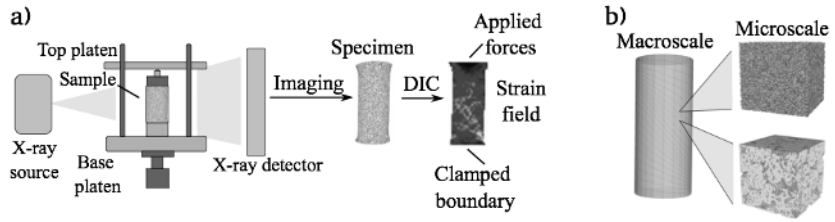

Figure 1.3. *(a) Identification of material datasets from in situ experiment. (b) Material datasets extracted from micromechanical RVEs, with examples showing a granular ensemble and a porous rock*

Homogenization of granular ensemblies

In the case where *discrete* element simulations (e.g. Karapiperis et al. (2020b)) are used for the purpose of generating the data, then the macroscopic material states (stress, strain, free energy, dissipation, and microstructural variables) need to be obtained from the discrete quantities (particle displacements and interparticle forces). Assuming quasi-static conditions, the average stress tensor of the granular assembly is given by Christoffersen et al. (1981):

$$\boldsymbol{\sigma} = \frac{1}{V} \sum_{c} \mathbf{f}^c \otimes \mathbf{l}^c \qquad [1.30]$$

where the summation is performed over all contacts c of all particles in the assembly (unit cell), $\mathbf{f}^c$ is the interparticle force, $\mathbf{l}^c$ is the branch vector connecting the centroids of contacting particles and V is the volume of the granular assembly. The average strain $\boldsymbol{\varepsilon}$ is obtained from the boundary deformation of the unit cell, and the free energy density due to local deformation at the contacts is given by:

$$\mathcal{A} = \sum_{c} \mathcal{A}^c = \frac{1}{2V} \sum_{c} \left(\frac{\|\mathbf{f}_n^c\|^2}{k_n} + \frac{\|\mathbf{f}_t^c\|^2}{k_t} \right) \qquad [1.31]$$

where k_n, k_t are the normal and tangential contact stiffnesses at an interparticle frictional contact, respectively, and $\mathbf{f}_n^c, \mathbf{f}_t^c$ are the normal and tangential components of the interparticle force.

The dissipation can be computed incrementally by energy balance:

$$d\mathcal{D} = \boldsymbol{\sigma} : d\boldsymbol{\varepsilon} - d\mathcal{A} \qquad [1.32]$$

or, from the frictional slip at the interparticle contacts:

$$d\mathcal{D} = \sum_{c} d\mathcal{D}^c = \frac{1}{V} \sum_{c} \mathbf{f}_t^c \cdot d\mathbf{u}^{c,\,\mathrm{slip}} \qquad [1.33]$$

where $d\mathbf{u}^{c,\,\mathrm{slip}} = (\mathbf{f}_t^{c,t} - \mathbf{f}_t^{c,t+dt})/k_t$.

Microstructural measures acting as internal variables augmenting the state space (section 2.3) may similarly be obtained by averaging microscopic quantities. For example, the commonly used contact normal fabric tensor (Oda 1972):

$$\boldsymbol{F} = \frac{1}{2N_c} \sum_{c} \boldsymbol{n}^c \otimes \boldsymbol{n}^c \qquad [1.34]$$

where N_c is the number of contacts in the assembly and $\boldsymbol{n}^c$ is the contact normal vector. Analogous quantities can be obtained for non-simple (polar) continua, as discussed in Karapiperis et al. (2021).

Homogenization of heterogeneous porous geomaterials

In the case where *continuum* microstructural RVEs are used to generate material datasets, then similar principles apply. Assuming quasistatic conditions, the average stress tensor of the micromechanical RVE is given as:

$$\boldsymbol{\sigma} = \frac{1}{V} \int_{\partial V} \mathbf{t} \otimes \mathbf{x} \, dS \qquad [1.35]$$

where $\mathbf{t}$ denotes the traction acting on the boundary of the continuum RVE and $\mathbf{x}$ denotes the position of the material point on the boundary.

The free energy and dissipation are given simply by averaging and energy balance, respectively:

$$\mathcal{A} = \int_V \mathcal{A}(\mathbf{x}) \, d\mathbf{x} \qquad [1.36]$$

$$d\mathcal{D} = \boldsymbol{\sigma} : d\boldsymbol{\varepsilon} - d\mathcal{A} \qquad [1.37]$$

while continuum texture tensors, similar to equation [1.34], may analogously be defined.

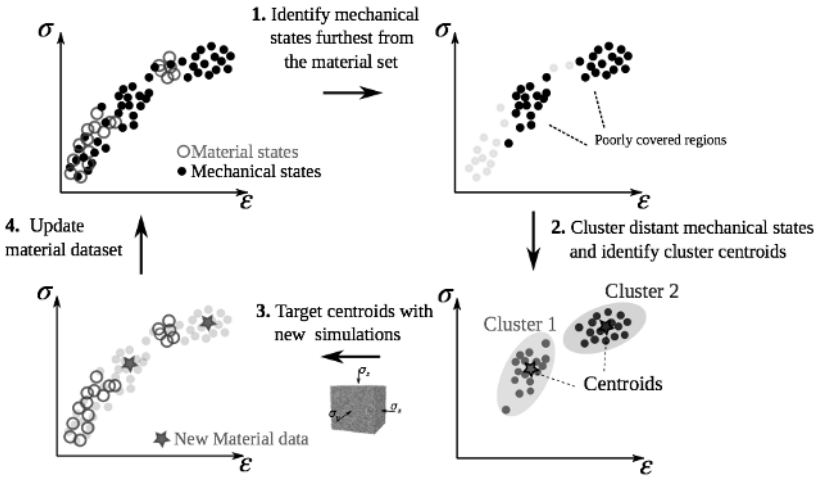

Figure 1.4. *Adaptive sampling procedure for multiscale data-driven computational mechanics*

Adaptive sampling

In the above, it was assumed that micromechanical calculations are carried out along predetermined stress paths. In practice, these predetermined paths may not sufficiently cover the state space as needed for a specific application or boundary value problem. In this case, we can leverage the formulation of data-driven computational mechanics as a distance minimization problem, and identify, using unsupervised learning, regions in state space with such poor data coverage. As shown in Figure 1.4, these regions may then be targeted with additional experiments or lower scale simulations, in an active learning manner. The result is a better coverage of the phase space for a given application or problem. The interested reader is referred to Gorgogianni et al. (2023) for details on this adaptive sampling technique.

1.3. Applications

We present here two representative examples that leverage the theoretical and algorithmic developments discussed above. The first one is a 2D flat punch indentation of an elastic medium, as shown in Figure 1.5(a). The lateral and lower boundaries remain fixed, while the upper surface is traction free, with the exception of the flat indenter that is driven downwards with a constant rate of displacement. The domain is discretized by means of bilinear quadrilateral elements. For simplicity, we restrict our attention to a simple and history-independent material behavior by generating a dataset of $N = 10^6$ stress–strain pairs via evaluating an isotropic linear elastic law of a model material with Young's modulus $E = 1.0$ MPa and Poisson's ratio $\nu = 0.3$. This allows us to use the formulation of section 1.2.1, where the constitutive law is entirely replaced by the aforementioned discrete dataset. We in fact repeat the prediction using a sequence of successively larger datasets, until convergence of the predicted response was obtained. This convergence can be verified in Figure 1.5(b). where the indenter force–displacement relation is plotted for increasing dataset size. The code needed to reproduce the

example is openly available in the author's Github repository (github.com/kkarapiperis/ddcm-2D/).

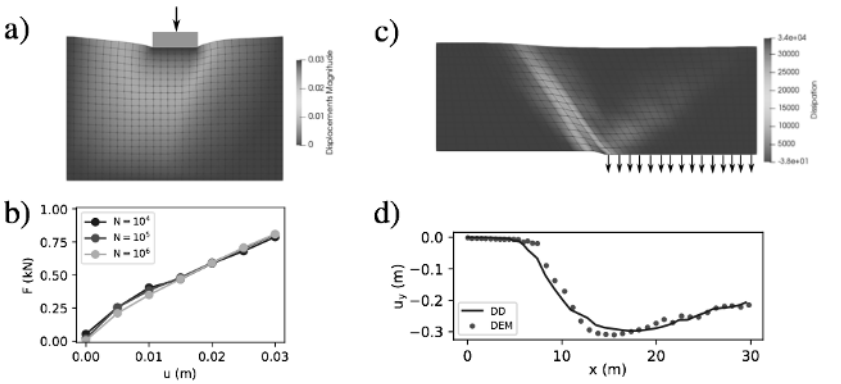

Figure 1.5. *(a) Example of a 2D flat punch indentation into an elastic medium. (b) Indenter force–displacement curve prediction for increasing size of the dataset. (c) Example of a fault rupture through a layer of model granular material. (d) Predicted surface displacement profile, and comparison with a fully resolved discrete element simulation*

In the second example, as shown in Figure 1.5(c). a rupture propagates into a model granular material. The left boundary and the left half of the lower boundary remain fixed, while the respective right part of the boundary is being displaced downwards at a constant rate, leading to a normal fault rupture. Similarly to the previous example, the domain is discretized by means of bilinear quadrilateral elements. Utilizing the history-dependent formulation of section 1.2.3, the constitutive law is replaced by a dataset originating from the homogenized response of a subangular 2D granular material, as shown in Figure 1.1(a). We extract this dataset by calculating the homogenized response (see section 1.2.4) at spatially distributed sampling location of a level-set discrete element simulation of the problem (Kawamoto et al. 2016; Feldfogel et al. 2023). The latter involves roughly 40,000 particles interacting via a frictional Coulomb law with an interparticle friction coefficient of $\mu = 0.5$. Upon sampling, this process results in a dataset with $6,000$ data points. The simulation shows a primary rupture to the left and an antithetic secondary rupture to the right, in accordance with similar observations

in experiments (Andò et al. 2007). Finally, the resulting surface deformation profile at the end of the simulation is shown in Figure 1.5(d). which compares well with a fully resolved discrete element simulation of the same problem.

1.4. Conclusions

In summary, the framework of data-driven computational mechanics offers a novel avenue to solve problems in geomechanics, including challenging ones that involve failure and localized deformation. Free from the uncertainty of the classical constitutive modeling approach and the caveats of ML models, the data-driven formulation offers an alternative paradigm for computation. The method is also readily extendable to dynamics (Kirchdoerfer and Ortiz 2018; Garcia-Suarez et al. 2023) and finite deformation (Conti et al. 2020). It would be interesting to explore the framework's performance in the presence of bifurcations and loss of uniqueness in the material response, as often observed in geomechanical problems. Finally, the need for large amounts of data represents a potential pitfall of the method, which may be addressed by the use of high-fidelity micromechanical simulations, augmenting datasets available from experiments, as well as through as the use of adaptive sampling techniques.

1.5. References

Anastasopoulos, I., Gazetas, G., Bransby, M.F., Davis, M.C.R., Nahas, A.E. (2007). Fault rupture propagation through sand: Finite-element analysis and validation through centrifuge experiments. *Journal of Geotechnical and Geoenvironmental Engineering*, 133(8), 943–958. doi: 10.1061/(ASCE)1090-0241(2007)133:8(943).

Andò, E., Hall, S., Viggiani, G., Desrues, J., Bésuelle, P. (2012). Grain-scale experimental investigation of localised deformation in sand: A discrete particle tracking approach. *Acta Geotechnica*, 7(1), 1–13. doi: 10.1007/s11440-011-0151-6.

Andrade, J.E. and Tu, X. (2009). Multiscale framework for behavior prediction in granular media. *Mechanics of Materials*, 41(6), 652–669 [Online]. Available at: http://www.sciencedirect.com/science/article/pii/S0167663608001737.

Bahmani, B. and Sun, W. (2021). A kd-tree-accelerated hybrid data-driven/model-based approach for poroelasticity problems with multi-fidelity multi-physics data. *Computer Methods in Applied Mechanics and Engineering*, 382, 113868.

Bahmani, B. and Sun, W. (2022). Manifold embedding data-driven mechanics. *Journal of the Mechanics and Physics of Solids*, 166, 104927.

Bardet, J. (1994). Numerical simulations of the incremental responses of idealized granular materials. *International Journal of Plasticity*, 10(8), 879–908 [Online]. Available at: http://www.sciencedirect.com/science/article/pii/0749641994900191.

Borja, R.I. and Andrade, J.E. (2006). Critical state plasticity. Part VI: Meso-scale finite element simulation of strain localization in discrete granular materials. *Computer Methods in Applied Mechanics and Engineering*, 195(37), 5115–5140 [Online]. Available at: http://www.sciencedirect.com/science/article/pii/S0045782505005402

Carrara, P., De Lorenzis, L., Stainier, L., Ortiz, M. (2020). Data-driven fracture mechanics. *Computer Methods in Applied Mechanics and Engineering*, 372, 113390.

Christoffersen, J., Mehrabadi, M.M., Nemat-Nasser, S. (1981). A micromechanical description of granular material behavior. *Journal of Applied Mechanics*, 48(2), 339–344.

Conti, S., Muller, S., Ortiz, M. (2020). Data-driven finite elasticity. *Archive for Rational Mechanics and Analysis*, 237(1), 1–33. doi: 10.1007/s00205-020-01490-x.

Cundall, P.A. and Strack, O.D.L. (1979). A discrete numerical model for granular assemblies. *Géotechnique*, 29(1), 47–65. doi: 10.1680/geot.1979.29.1.47.

Dafalias, Y.F. and Manzari, M.T. (2004). Simple plasticity sand model accounting for fabric change effects. *Journal of Engineering Mechanics*, 130(6), 622–634. doi: 10.1061/(ASCE)0733-9399 (2004)130:6(622).

Darve, F. and Labanieh, S. (1982). Incremental constitutive law for sands and clays: Simulations of monotonic and cyclic tests. *International Journal for Numerical and Analytical Methods in Geomechanics*, 6(2), 243–275. doi: 10.1002/nag.1610060209.

Darve, F. and Nicot, F. (2005). On incremental non-linearity in granular media: Phenomenological and multi-scale views (Part I). *International Journal for Numerical and Analytical Methods in Geomechanics*, 29(14), 1387–1409. doi: 10.1002/nag.466.

Eggersmann, R., Kirchdoerfer, T., Reese, S., Stainier, L., Ortiz, M. (2019). Model-free data-driven inelasticity. *Computer Methods in Applied Mechanics and Engineering*, 350, 81–99 [Online]. Available at: http://www.sciencedirect.com/science/article/pii/S0045782519300878.

Eggersmann, R., Stainier, L., Ortiz, M., Reese, S. (2021). Model-free data-driven computamechanics enhanced by tensor voting. *Computer Methods in Applied Mechanics and Engineering*, 373, 113499.

Eghbalian, M., Pouragha, M., Wan, R. (2022). A physics-informed deep neural network for surrogate modeling in classical elasto-plasticity. *arXiv*. doi: 10.48550/arXiv.2204.12088.

Feldfogel, S., Karapiperis, K., Andrade, J.E., Kamemr D.S. (2023). A discretization-convergent level-set-discrete-element-method using a continuum-based contact formulation. *International Journal for Numerical Methods in Engineering*, e7400. doi: 10.1002/nme.7400.

Garcia-Suarez, J., Cornet, A., Wattel, S., Molinari, J.-F. (2023). Data-driven 1D wave propagation for site response analysis. *International Journal for Numerical and Analytical Methods in Geomechanics*, 47(15), 2691–2705.

Gorgogianni, A., Karapiperis, K., Stainier, L., Ortiz, M., Andrade, J.E. (2023). Adaptive goal-oriented data sampling in data-driven computational mechanics. *Computer Methods in Applied Mechanics and Engineering*, 409, 115949.

Guo, N. and Zhao, J. (2014). A coupled fem/dem approach for hierarchical multiscale modelling of granular media. *International Journal for Numerical Methods in Engineering*, 99(11), 789–818. doi: 10.1002/nme.4702.

Haghighat, E., Raissi, M., Moure, A., Gomez, H., Juanes, R. (2021). A physics-informed deep learning framework for inversion and surrogate modeling in solid mechanics. *Computer Methods in Applied Mechanics and Engineering*, 379, 113741.

Haghighat, E., Abouali, S., Vaziri, R. (2023). Constitutive model characterization and discovery using physics-informed deep learning. *Engineering Applications of Artificial Intelligence*, 120, 105828.

Hall, S., Bornert, M., Desrues, J., Pannier, Y., Lenoir, N., Viggiani, G., Bésuelle, P. (2010). Discrete and continuum analysis of localised deformation in sand using X-ray CT and volumetric digital image correlation. *Géotechnique*, 60(5), 315–322. doi: 10.1680/geot.2010.60.5.315.

Houlsby, G.T. and Puzrin, A.M. (2006). *Principles of Hyperplasticity*. Springer, London.

Huang, S., He, Z., Reina, C. (2022). Variational onsager neural networks (VONNs): A thermodynamics-based variational learning strategy for non-equilibrium PDEs. *Journal of the Mechanics and Physics of Solids*, 163, 104856.

Kamrin, K., Rycroft, C., Bazant, M.Z. (2007). The stochastic flow rule: A multi-scale model for granular plasticity. *Modelling and Simulation in Materials Science and Engineering*, 15(4), S449 [Online]. Available at: http://stacks.iop.org/0965-0393/15/i=4/a=S10.

Karapiperis, K., Harmon, J., Andò, E., Viggiani, G., Andrade, J.E. (2020a). Investigating the incremental behavior of granular materials with the level-set discrete element method. *Journal of the Mechanics and Physics of Solids*, 144, 104103 [Online]. Available at: http://www.sciencedirect.com/science/article/pii/S0022509620303379.

Karapiperis, K., Stainier, L., Ortiz, M., Andrade, J. (2020b). Data-driven multiscale modeling in mechanics. *Journal of the Mechanics and Physics of Solids*, 104239 [Online]. Available at: http://www.sciencedirect.com/science/article/pii/S0022509620304531.

Karapiperis, K., Ortiz, M., Andrade, J. (2021). Data-driven nonlocal mechanics: Discovering the internal length scales of materials. *Computer Methods in Applied Mechanics and Engineering*, 386, 114039 [Online]. Available at: https://www.sciencedirect.com/science/article/pii/ S0045782521003704.

Kawamoto, R., Andò, E., Viggiani, G., Andrade, J.E. (2016). Level set discrete element method for three-dimensional computations with triaxial case study. *Journal of the Mechanics and Physics of Solids*, 91, 1–13. doi: 10.1016/j.jmps.2016.02.021.

Kawamoto, R., Andò, E., Viggiani, G., Andrade, J.E. (2018). All you need is shape: Predicting shear banding in sand with LS-DEM. *Journal of the Mechanics and Physics of Solids*, 111, 375–392 [Online]. Available at: http://www.sciencedirect.com/science/article/pii/S0022509617306580.

Kirchdoerfer, T. and Ortiz, M. (2016). Data-driven computational mechanics. *Computer Methods in Applied Mechanics and Engineering*, 304, 81–101 [Online]. Available at: http://www.sciencedirect.com/science/article/pii/S0045782516300238.

Kirchdoerfer, T. and Ortiz, M. (2018). Data-driven computing in dynamics. *International Journal for Numerical Methods in Engineering*, 113(11), 1697–1710. doi: 10.1002/nme.5716.

Leygue, A., Coret, M., Rethore, J., Stainier, L., Verron, E. (2018). Data-based derivation of material response. *Computer Methods in Applied Mechanics and Engineering*, 331, 184–196 [Online]. Available at: http://www.sciencedirect.com/science/article/pii/S0045782517307156.

Masi, F., Stefanou, I., Vannucci, P., Maffi-Berthier, V. (2021). Thermodynamics-based artificial neural networks for constitutive modeling. *Journal of the Mechanics and Physics of Solids*, 147, 104277.

Mühlhaus, H.-B. and Alfantis, E. (1991). A variational principle for gradient plasticity. *International Journal of Solids and Structures*, 28(7), 845–857 [Online]. Available at: http://www.sciencedirect.com/science/article/pii/002076839190004Y.

Mühlhaus, H.B. and Vardoulakis, I. (1987). The thickness of shear bands in granular materials. *Géotechnique*, 37(3), 271–283. doi: 10.1680/geot.1987.37.3.271.

Nicot, F., Darve, F., RNVO Group: Natural Hazards and Vulnerability of Structures. (2005). A multi-scale approach to granular materials. *Mechanics of Materials*, 37(9), 980–1006 [Online]. Available at: http://www.sciencedirect.com/science/article/pii/S016766360400167X.

Oda, M. (1972). Initial fabrics and their relation to mechanical properties of granular materials. *Soils and Foundations*, 12(1), 17–36.

Ortiz, M. and Pandolfi, A. (2004). A variational cam-clay theory of plasticity. *Computer Methods in Applied Mechanics and Engineering*, 193(27), 2645–2666 [Online]. Available at: http://www.sciencedirect.com/science/article/pii/S00457825040 00817.

Prume, E., Reese, S., Ortiz, M. (2023). Model-free data-driven inference in computational mechanics. *Computer Methods in Applied Mechanics and Engineering*, 403, 115704.

Regueiro, R.A. and Yan, B. (2011). Concurrent multiscale computational modeling for dense dry granular materials interfacing deformable solid bodies. In *Bifurcations, Instabilities and Degradations in Geomaterials*, Wan, R., Alsaleh, M., Labuz, J. (eds). Springer, Berlin, Heidelberg.

Roscoe, K.H. (1970). The influence of strains in soil mechanics. *Géotechnique*, 20(2), 129–170. doi: 10.1680/geot.1970.20.2.129.

Roscoe, K.H., Schofield, A.N., Wroth, C.P. (1958). On the yielding of soils. *Géotechnique*, 8(1), 22–53. doi: 10.1680/geot.1958.8.1.22.

Ulloa, J., Gorgogianni, A., Karapiperis, K., Ortiz, M., Andrade, J.E. (2023). Data-driven breakage mechanics: Predicting the evolution of particle-size distribution in granular media. *Journal of the Mechanics and Physics of Solids*, 178, 105328.

Vardoulakis, I. and Aifantis, E. (1991). A gradient flow theory of plasticity for granular materials. *Acta Mechanica*, 87(3), 197–217. doi: 10.1007/BF01299795.

Vlassis, N.N. and Sun, W. (2023). Geometric learning for computational mechanics part II: Graph embedding for interpretable multiscale plasticity. *Computer Methods in Applied Mechanics and Engineering*, 404, 115768.